B- and T-cell acute lymphoblastic leukemias evade chemotherapy at distinct sites in the bone marrow

Journal Article

Author(s):
Barz, Malwine J.; Behrmann, Lena; Capron, Danaëlle; Zuchtriegel, Gabriele; Steffen, Fabio D.; Kunz, Leo; Zhang, Yang; Vermeerbergen, Iria Jimenez; Marovca, Blerim; Kirschmann, Moritz; Zech, Antonia; Nombela-Arrieta, César; Ziegler, Urs; Schroeder, Timm; Bornhauser, Beat; Bourquin, Jean-Pierre

Publication date:
2023-05

Permanent link:
https://doi.org/10.3929/ethz-b-000612678

Originally published in:
Haematologica 108(5), https://doi.org/10.3324/haematol.2021.280451

Funding acknowledgement:
186271 - Elucidating the human mesenchymal bone marrow stromal hierarchy in health and disease (SNF)

B- and T-cell acute lymphoblastic leukemias evade chemotherapy at distinct sites in the bone marrow

Malwine J. Barz,[1*] Lena Behrmann,[1*] Danaëlle Capron,[1*] Gabriele Zuchtriegel,[1*] Fabio D. Steffen,[1] Leo Kunz,[2] Yang Zhang,[2] Iria Jimenez Vermeerbergen,[1] Blerim Marovca,[1] Moritz Kirschmann,[3] Antonia Zech,[1] César Nombela-Arrieta,[4] Urs Ziegler,[3] Timm Schroeder,[2] Beat Bornhauser[1] and Jean-Pierre Bourquin[1]

[1]University Children's Hospital Zürich, Pediatric Oncology and Children's Research Center, Balgrist Campus AG, Zürich; [2]ETH Zürich, Department of Biosystems Science and Engineering, Basel; [3]University of Zürich, Center for Microscopy and Image Analysis, Zürich and [4]University Hospital Zürich, Division of Hematology, Zürich, Switzerland

**MJB, LB, DC and GZ contributed equally and are listed in alphabetical order.*

Correspondence: J-P. Bourquin
jean-pierre.bourquin@kispi.uzh.ch

Received: December 2, 2021.
Accepted: October 14, 2022.
Early view: November 3, 2022.

https://doi.org/10.3324/haematol.2021.280451

Abstract

Persistence of residual disease after induction chemotherapy is a strong predictor of relapse in acute lymphoblastic leukemia (ALL). The bone marrow microenvironment may support escape from treatment. Using three-dimensional fluorescence imaging of ten primary ALL xenografts we identified sites of predilection in the bone marrow for resistance to induction with dexamethasone, vincristine and doxorubicin. We detected B-cell precursor ALL cells predominantly in the perisinusoidal space at early engraftment and after chemotherapy. The spatial distribution of T-ALL cells was more widespread with contacts to endosteum, nestin$^+$ pericytes and sinusoids. Dispersion of T-ALL cells in the bone marrow increased under chemotherapeutic pressure. A subset of slowly dividing ALL cells was transiently detected upon short-term chemotherapy, but not at residual disease after chemotherapy, challenging the notion that ALL cells escape treatment by direct induction of a dormant state in the niche. These lineage-dependent differences point to niche interactions that may be more specifically exploitable to improve treatment.

Introduction

Acute lymphoblastic leukemia (ALL) disseminates from transformed lymphoid progenitors that most likely arise in specific microenvironments, preferentially in the bone marrow, competing with normal hematopoiesis.[1,2] Persistence of minimal residual disease (MRD) under chemotherapy is a strong predictor of relapse,[3] but the underlying mechanisms that enable cells to escape treatment are still unclear. Non-oncogenic mechanisms of adaptation are likely to contribute to this bottleneck, in which interactions with the tumor microenvironment are thought to play important roles.[4] Hematopoietic stem cells (HSC) reside in the bone marrow in proximity to endosteal cells,[5] perivascular cells[6,7] and peripheral nerve fibers.[8] Sinusoidal endothelial networks may also contribute to the support of HSC at different locations.[9] Recent advances made in three-dimensional (3D) imaging enable comprehensive visualization and quantification of HSC in mouse models. These imaging studies challenge the notion that HSC are enriched in a specific neighborhood, where HSC localization is determined by microanatomical properties of the bone marrow structures, rather than active selection of niches by HSC.[10] Alternative roles were proposed in currently unexplored heterogeneous subsets of sinusoidal, perisinusoidal and stromal cells.[10] B-cell precursor (BCP) ALL cells are thought to compete with healthy HSC by hijacking normal homeostatic functions.[1,11] In a xenotransplantation model, human NALM-6 BCP-ALL cells interact with HSC at vascular sites expressing E-selectin and SDF-1 (CXCL12) and remodel the mesenchymal stromal compartment.[12,13] *Ex vivo*, co-cultures with mesenchymal stromal cells or endothelial cells maintain ALL cell survival.[14] The contribution of endothelial cells to a leukemia niche remains unclear and was challenged recently by experiments with ALL xenografts, which suggested the persistence of so-called dormant ALL cells after treatment with cytarabine. These cells localize to the endosteum and constitute a potentially reversible quiescent MRD state.[15] Clinical observations suggest relevant differences between BCP-ALL and T-ALL with respect to sites of predilection to chemotherapy-resistant states in MRD.[16] While MRD levels do not correlate well between peripheral blood and bone marrow in BCP-ALL, MRD levels are comparable in the two compartments in patients with T-ALL.[16] This may explain discrepant observations reported with mouse models, in addition to species-related differences. Contradicting previous studies

using NALM-6 cells, *in vivo* imaging of a genetically engineered mouse model of NOTCH-mutated T-ALL revealed that T-ALL cells were highly mobile and cycling even after exposure to chemotherapy. No preferential sub-localization within the bone marrow space was observed,[17] challenging the notion that T-ALL may escape chemotherapy in a dormant leukemia niche. These observations indicate that patterns of interaction of leukemia cells with their microenvironment may be more heterogeneous than previously thought.

Leukemia patient-derived xenografts (PDX) using NOD.Cg-*Prkdc*$_{scid}$ *IL2rg*$_{tm1Wjl}$/SzJ (NSG) mice often reliably mirror the clonal composition and phenotype of the corresponding patients' samples.[18,19] Using 3D confocal fluorescence microscopy, we studied the topology of MRD in the bone marrow after induction treatment, in a variety of primary human high risk BCP- and T-ALL subtypes. We found that BCP-ALL cells engraft and persist preferentially in close proximity to extravascular endothelial sinusoids in the bone marrow, while T-ALL cells have a more widespread distribution including contacts with the endosteal lining, underscoring the highly dynamic mobility of T-ALL in comparison to BCP-ALL. We provide a detailed comparison of engraftment and chemotherapy survival behavior of BCP- and T-ALL, revealing important differences between these leukemic entities. This encourages critical investigation of interactions between leukemic blasts and niche cells to identify druggable pathways for clinical treatments.

Methods

Primary samples

Patients' samples were obtained with the written informed consent of the patients' parents or legal guardians in accordance with the Declaration of Helsinki and approval was granted by the ethics commission of the Canton of Zürich (approval number 2014-0383). Xenografts were recovered from cryopreserved bone marrow aspirates of patients enrolled in the ALL-BFM 2000 and 2009 and ALL-REZ BFM 2002 studies.

Xenotransplantation

NSG and C57BL/6J mice were obtained from The Jackson Laboratory. Xenotransplantation of ALL samples was performed by intravenous injection into unconditioned 6- to 8-week-old mice in accordance with animal care regulations after approval by legal authorities (125/2013, 124/16, 131/19). For *in vivo* bioluminescence imaging, the mice were anesthetized, given an intravenous injection of D-luciferin and imaged. Cell proliferation of leukemic cells was traced *in vivo* using 5(6)-carboxyfluorescein diacetate N-succinimidyl ester (CFSE). Details are provided in the *Online Supplementary Methods*.

Lentiviruses

pSLIG (SFFV-Luc2-IRES-eGFP), pMD2.G and psPAX2 plasmids were used to generate luciferase-expressing lentiviruses. PDX cells were transduced with the lentiviruses and expanded in NSG mice for re-transplantation, as described in the *Online Supplementary Methods*.

Flow cytometry

Human engraftment was determined in bone marrow harvested from tibiae or femora. Human engraftment was monitored as the percentage of human cells over all human (anti-human-CD19 PE [BioLegend]; anti-human-CD7 PE [ebiosciences]; anti-human-CD45 Alexa Fluor 647 [BioLegend]) and murine leukocytes (anti-mouse-CD45 eFluor 450, [ebiosciences]) (*Online Supplementary Methods*).

Drug response profiling

Leukemia cells from PDX samples were co-cultured with mesenchymal stromal cells for 24 h in 384-well plates, treated with chemotherapeutic drugs for 72 h and imaged using high-throughput fluorescence microscopy. Drug response profiles were determined by fitting a three-parameter, dose-response model (log IC_{50}, I_{max} and n) to dimethylsulfoxide-normalized cell counts.

Three-dimensional confocal imaging of bones

Bones were fixed, snap-frozen and cut using a Cryostat for thick sections. Sectioned bones were blocked, stained with primary (anti-human-CD45 [MEM-28], anti-mouse-endoglin [AF1320], anti-mouse-perilipin [D1D8], anti-mouse-laminin [L9393], anti-mouse-collagen type I [CL50151AP], anti-mouse-endomucin [V.7C7], anti-mouse-osterix [NBP2-38019]) and secondary antibodies and embedded in RapiClear for imaging. Sinusoids were defined as endoglin^{+} or endoglin^{high}endomucin^{low}, transition zones as endoglin^{low}endomucin^{high}, and nestin-associated vessels as nestin-GFP^{+}endomucin^{-}endoglin^{-}. The endosteal space was set as collagen type I-positive structures or delimited using DAPI and osterix co-staining. Leukemic cells were defined as hCD45^{+} cells with a round morphology. Tiled z-stack images were acquired using a Leica SP8 inverse microscope.

Distance analysis and random dots

The 3D confocal images were analyzed quantitatively by measuring the spatial proximity between leukemic cells and bone marrow sinusoids or bone using Imaris. First, all imaged channels were preprocessed with a Gaussian filter to remove noise and signals were normalized slice-wise by the mean intensity to account for intensity loss along the z-axis. Leukemic cells were segmented using the hCD45 signal, while vascular surfaces were identified with the endoglin, endomucin or nestin signal by thresholding.

Bone structures were either segmented from DAPI-negative regions delimited with the osterix signal or from the collagen 1a signal. The masks for surfaces and spots were curated to reduce staining noise by removing small, unconnected objects with a size threshold based on voxel number. Volumes of the vessels, bones and the combined tissue map (leukemic cells, vasculature and bone) were filled separately with an image closing operation, i.e. dilation followed by erosion. Subsequently, the Euclidean distance transformation of the binary blood vessel or bone mask was computed using *bwdist* in Matlab.[20] The transformation provides a distance map of each voxel in the tissue to the nearest voxel of the vasculature or bone mask. The smallest distance of all voxels belonging to a leukemic cell was recorded from the distance map and plotted as histograms. Random virtual cells (random dots) with the same dimensions as the segmented leukemia cells were seeded in the tissue outside of the blood vessels and bones using XiT.[21] Specifically, a virtual cell was accepted if the coordinates of the centroid, sampled from a uniform distribution, was within the tissue region but outside of the masked blood vessel or bone structures. Otherwise, the virtual cell position was discarded and the random dot generation was iterated until the total number of leukemic cells in the image was reached. Minimum distances to blood vessel and bone surfaces were inferred as for real leukemic cells. The spatial distribution of leukemic cells were then compared to the randomly dispersed virtual cells. Enrichment of leukemic cells near the vasculature and/or bone was quantified as binwise fold-changes of hCD45$^+$ cells over random dots. Bins containing less than ten random dots were omitted from analysis.

Statistics

Differences between distributions were assessed by a two-tailed Kolmogorov-Smirnov test. Medians as well as individual bins were analyzed using a two-tailed Mann-Whitney U test. *P* values <0.05 were considered statistically significant. Statistical analyses were performed using GraphPad Prism (version 5.04) and SciPy (version 1.7.1).

Results

A leukemia xenograft model of induction chemotherapy in acute lymphoblastic leukemia to study minimal residual disease

To study the topology of resistant disease we established a model of induction chemotherapy using primary human leukemia cells derived from nine pediatric BCP-ALL and five T-ALL patients in NSG mice (Figure 1A; *Online Supplementary Table S1*). Luciferase-positive ALL cells were detected as early as 1 day after transplantation in the femora by bioluminescence imaging (Figure 1B). This supports the notion of the bone marrow as a favorable environment for ALL engraftment. We detected preferential colonization in distinct foci of the proximal and distal metaphyses and epiphyses (Figure 1C). By sequential flow cytometry analysis, leukemic cells were first detected in the bone marrow, subsequently in the spleen and later in the peripheral blood (Figure 1D) with similar kinetics of progression (Figure 1E). To study MRD, we established a 28-day three-drug chemotherapy regimen, combining three out of four drugs of the AIEOP-BFM ALL induction regimen, administering dexamethasone, doxorubicin, and vincristine (Figure 1A).[12,22] Animals were treated with this combination beginning on day 11 after transplantation, resulting in responses with detectable residual disease 32 days after initiation of therapy (Figure 1F-H). Reduction of the leukemic burden after induction treatment *in vivo* was detected in different ALL subtypes (*Online Supplementary Table S1*). Differences in residual extramedullary involvement were found in the model, in which one PDX showed particularly high leukemia burden in the liver compared to the bone marrow (Figure 1I). In all cases we detected residual cells in the spleen and brain after therapy. We observed involvement of the CNS in 24 independent PDX models (*Online Supplementary Figure S1*; *Online Supplementary Table S2*) as also reported previously by others,[23,24] and consistent with the well-documented clinical need for intrathecal chemotherapy to prevent relapses in ALL. Between 7 to 28 days after the end of induction, chemotherapy-resistant leukemic cells repopulated the bone marrow leading to relapse. We used our PDX model to chart the spatial organization of leukemic cells in the bone marrow and characterize the niches of MRD *in vivo*.

B- and T-cell acute lymphoblastic leukemia cells preferentially localize perisinusoidally at early engraftment

To define the predilection sites of leukemic cells in the bone marrow, we performed 3D confocal imaging of leukemic cells in murine bone marrow. Engraftment of ALL cells was observed in femora, tibiae, tail and sternum (*Online Supplementary Figure S2*). Femora were used to quantitatively assess the spatial distribution of ALL cells within the bone marrow microenvironment. To this end, we segmented leukemic cells (anti-human CD45), the host vasculature (anti-mouse endoglin) as well as the bone (collagen I or osterix) and computed a distance isomap around the vasculature (Figure 2A). We visualized engraftment of BCP-ALL and T-ALL cells in the bone marrow at day 11 and day 4, respectively (Figure 2B, C). In order to normalize the unique architectural constraints of each individual bone, we computationally seeded random dots throughout the bone marrow volume, excluding bone ma-

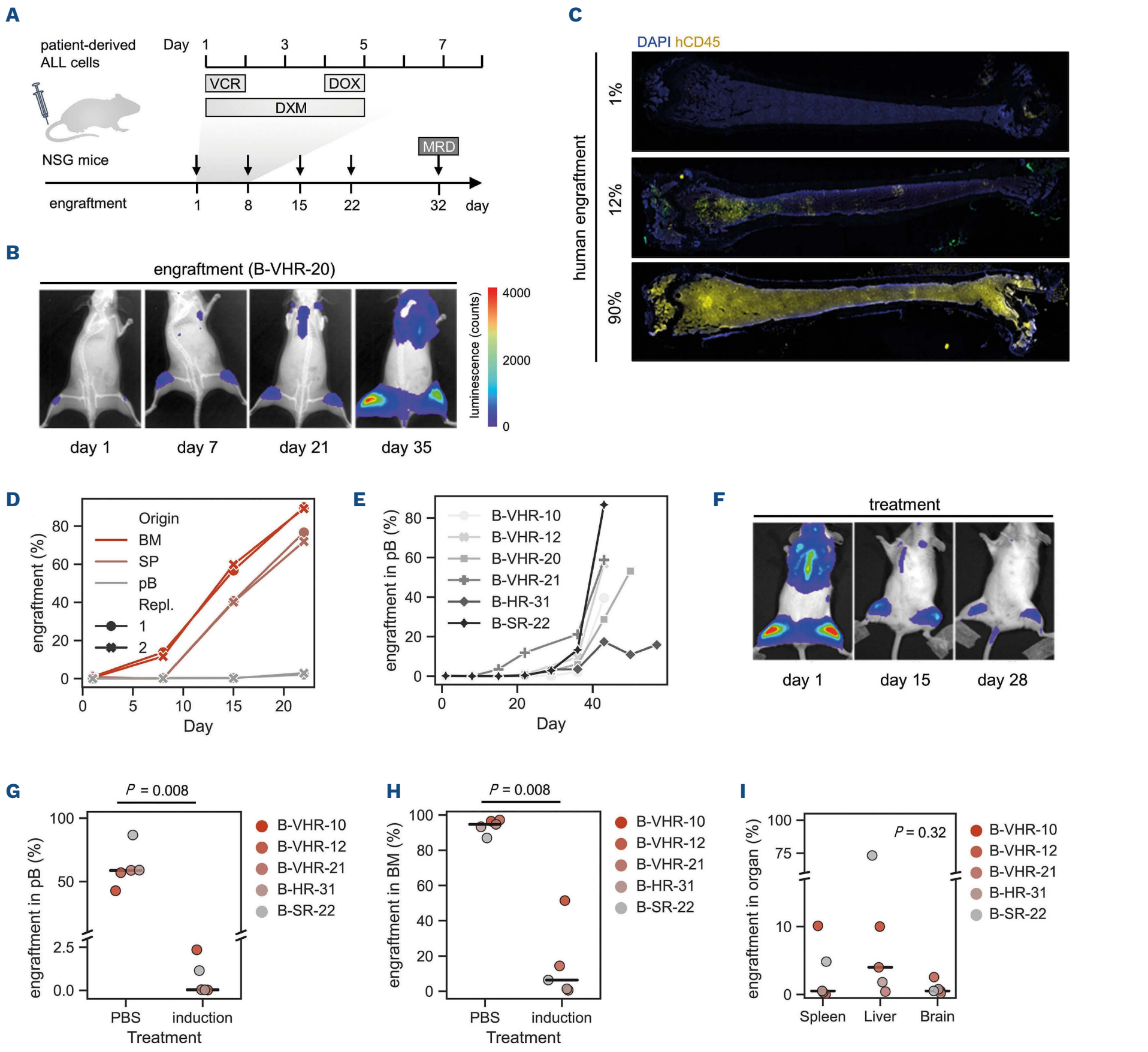

Figure 1. *In vivo* xenotransplantation model for engraftment and minimal residual disease in B-cell precursor acute lymphoblastic leukemia reflects the clinical situation of standard and very high-risk patients. (A) Xenotransplantation protocol of human leukemia cells derived from B-cell precursor acute lymphoblastic leukemia (ALL) and T-ALL patients' material into NSG mice. For three-drug chemotherapy mice were treated for 28 days with vincristine 0.5 mg/kg weekly on day 1, doxorubicin 2 mg/kg on day 4, and dexamethasone 10.5 mg/kg on days 1-5. The response to treatment was assessed on day 32 after initiation of therapy. (B) Disease progression of B-VHR-20 visualized by *in vivo* bioluminescence imaging of the total body. (C) Low magnification tiles (5x) from 15 μm thin sections of femora of mice at low, medium and high engraftment (DAPI, blue, indicates nuclei; hCD45$^+$, yellow, indicates leukemic cells). (D) Flow cytometry of bone marrow, spleen, and peripheral blood, each symbol representing data from a single mouse transplanted with B-VHR-20. (E) Progression of hCD45$^+$ cells in the peripheral blood visualized by flow cytometry of further B-cell precursor ALL. (F) Monitoring of chemotherapy response of B-VHR-20 via *in vivo* bioluminescence imaging and (G) flow cytometry analysis of hCD45$^+$ cells in peripheral blood and (H) bone marrow 32 days after initiation of combination chemotherapy. Medians were compared by a two-tailed Mann-Whitney U test. (I) Flow cytometry analysis of hCD45$^+$ engraftment in spleen, liver and brain upon induction treatment; each symbol represents data from one animal (1 mouse per patient's material, 2-tailed Kruskal-Wallis test). The percentage of human engraftment was calculated in relation to the total leukocyte count (human CD45$^+$ plus murine CD45$^+$) in mice. VCR: vincristine; DOX: doxorubicin; DXM: dexamethasone; MRD: minimal residual disease; BM: bone marrow; SP: spleen; pB: peripheral blood; PBS: phosphate-buffered saline.

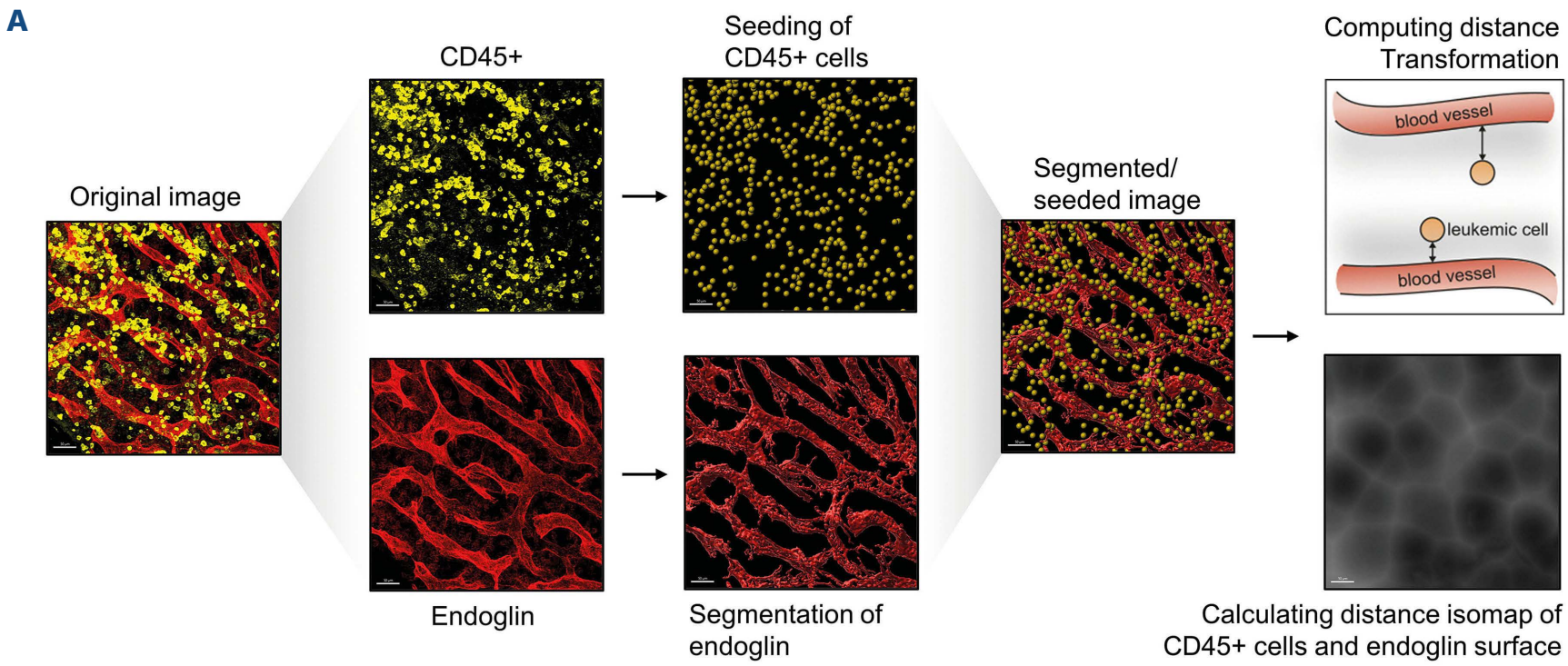

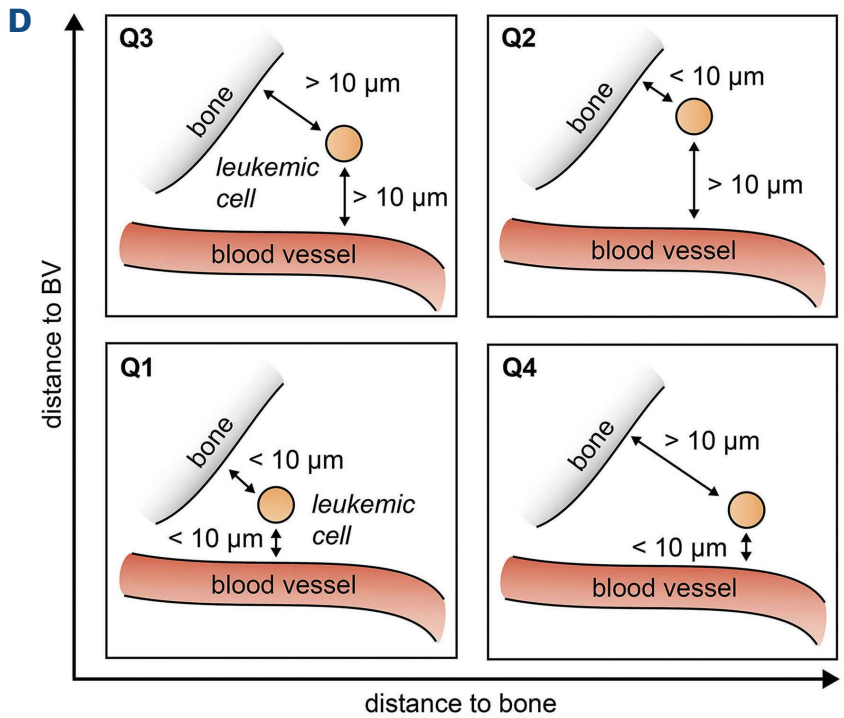

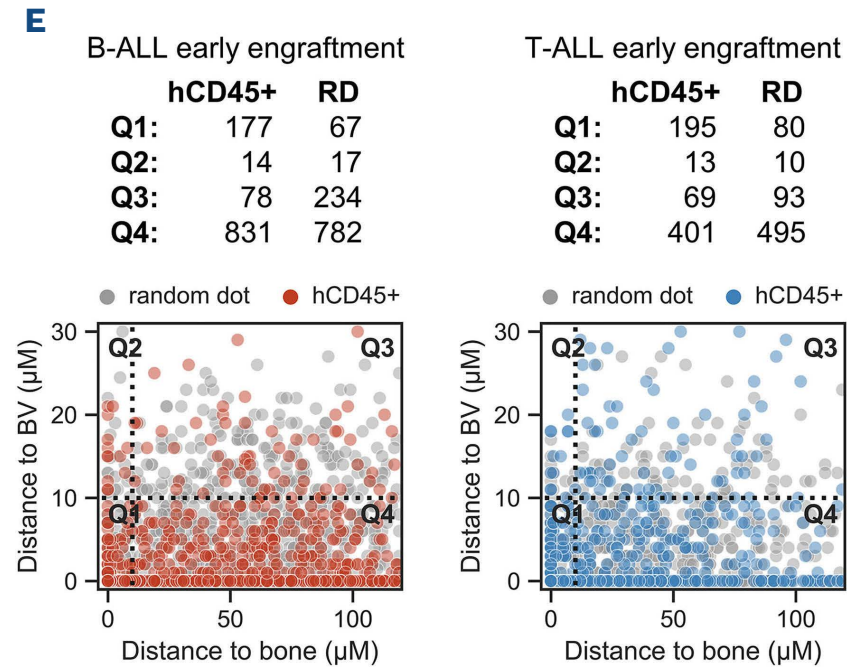

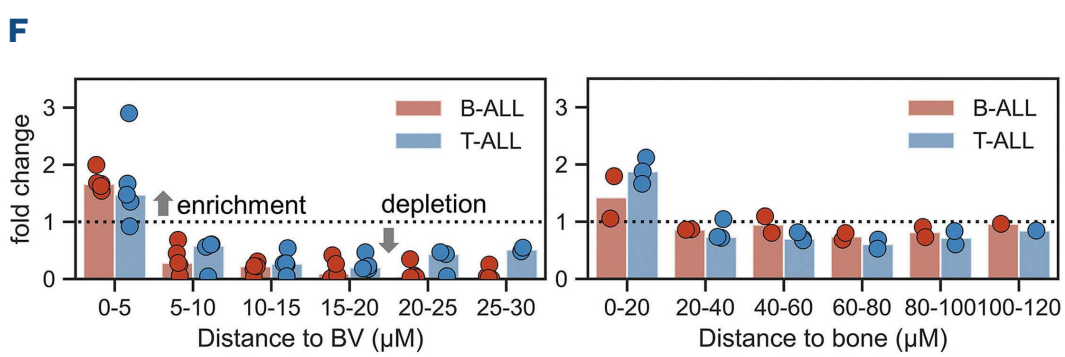

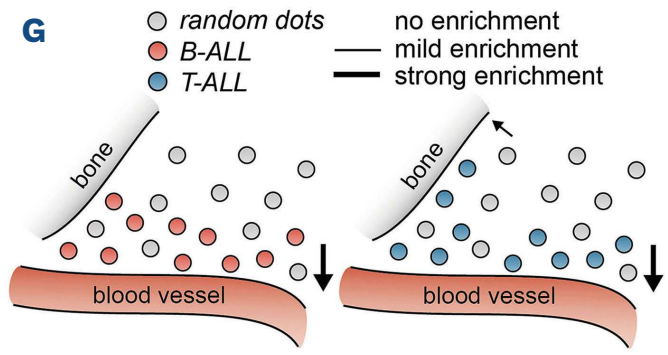

Continued on following page.

Figure 2. Distribution patterns of B-cell precursor acute lymphoblastic leukemia and T-acute lymphoblastic leukemia cells in the bone marrow microenvironment are similar at early engraftment. (A) Schematic representation of three-dimensional confocal microscopy followed by automated segmentation and quantitative distance analysis of early engrafted acute lymphoblastic leukemia (ALL): day 11 for B-cell precursor (BCP) ALL and day 4 for T-ALL (B, C). Representative maximal projection of a tiled 100-300 μm z-stack confocal image of patient-derived BCP- or T-ALL cells at early engraftment (B: B-R-03; C: T-VHR-09). Scale bars: 500 μm on overviews, 50 μm on zoomed images. Human leukemic cells (CD45$^+$, yellow) in spatial relationship with sinusoids (endoglin$^+$, red) or endosteum (collagen 1a$^+$, white). (D) Schematic categorization of individual leukemia cells into four quartiles based on their distance to bone and blood vessels. (E) Distribution of mean distances of BCP-ALL (red, B-R-03, B-SR-21 and B-VHR-24) or T-ALL (blue, T-HR-04, T-VHR-01 and T-VHR-04) cells to the bone and the bone marrow sinusoids at early engraftment (n=1,100 BCP-ALL segmented cells and n=678 T-ALL segmented cells). (F) Bar chart showing binwise fold-changes of BCP-ALL and T-ALL cells over random dots for distances to blood vessels (left panel) and bone (right panel). The data represented are pooled from three different bones transplanted with the same patient-derived BCP-ALL or T-ALL cells. (G) Schematic depiction of predilection sites of leukemic cells in the bone marrow. BV: blood vessel (bone marrow sinusoid); Q: quartile; h: human; RD, random dots.

trix and blood vessels. Mapping the distance of each leukemic cell or random dot to blood vessels and bone we assessed any preferential association of ALL cells to either niche. We dissected the resulting two-dimensional distance distribution into four quartiles by setting a threshold of 10 μm (distance quantiles Q1 to Q4), which is comparable to the size of an ALL cell (Figure 2D). Clustering of BCP-ALL and T-ALL cells close to bone marrow sinusoids was observed at early engraftment (<10 μm, Q1 and Q4, BCP-ALL P<0.001, T-ALL P=0.032) (Figure 2E; *Online Supplementary Figure S3A-D*). To quantify the enrichment of ALL cells we calculated binwise fold-changes of hCD45$^+$ cells over random dots. At early engraftment ALL cells localized strongly to blood vessels (<5 μm) (Figure 2F; *Online Supplementary Figure S3E, F*). In contrast to BCP-ALL, T-ALL cells were also strongly enriched in close vicinity to the bone (<24 μm) (Figure 2F; *Online Supplementary Figure S3G, H*), supporting the notion of different homing sites of BCP-ALL and T-ALL cells in the bone marrow (Figure 2G).

Upon chemotherapy T-cell acute lymphoblastic leukemia cells redistribute in the bone marrow

Next, we assessed the spatial reorganization of BCP-ALL and T-ALL cells after 28 days of induction therapy (Figures 1A and 3A, B). Upon drug perturbation, cells from different BCP-ALL patients were still found close to sinusoids (P<0.001, <10 μm, Q1 and Q4) (Figure 3C; *Online Supplementary Figure S4A-E*), whereas cells of T-ALL patients localized near the bone (P<0.001, <10 μm, Q1 and Q2) but their position did not differ from random dots with respect to blood vessels (P=ns; <10 μm, Q2 to Q4) (Figure 3C; *Online Supplementary Figure S4F, G*). Overall, BCP-ALL cells surviving chemotherapy resided close to endothelial blood vessels (Figure 3D; *Online Supplementary Figure S4H-J*). Chemotherapy-resisting T-ALL cells scattered more broadly in the bone marrow and were less enriched at the vasculature compared to early engraftment (Figure 3D; *Online Supplementary Figure S4K, L*), but maintained a preference for association with the endosteum. We conclude that the 28-day induction regimen induced different spatial localization of BCP-ALL and T-ALL cells, indicating immunophenotype-specific survival strategies within the microenvironment (Figure 3E).

T-cell acute lymphoblastic leukemia cells are closer to nestin-positive cells than are B-cell acute lymphoblastic leukemia cells

Given the relevance of the perivascular niche for leukemic engraftment and survival during chemotherapy we investigated the bone marrow vasculature in more detail. As shown by Asada *et al.*,[7] the vascular niche of HSC offers different perivascular cells, such as nestin$^+$ cells, which might interact with leukemic cells.[25] Using our established deep-tissue imaging, we studied the spatial relation of BCP-ALL and T-ALL cells with respect to nestin$^+$ cells by xenotransplantation of PDX samples in nestin-GFP transgenic mice (Figure 4A, B). At early engraftment, BCP-ALL cells showed a similar distribution as random dots to nestin$^+$ cells (Figure 4C; *Online Supplementary Figure S5*), whereas T-ALL cells were enriched at nestin$^+$ cells compared to a random distribution (<20 μm) (Figure 4D; *Online Supplementary Figure S5*). Consistent with NSG mice, BCP-ALL and T-ALL cells were found close to blood vessels, however T-ALL cells were more enriched at nestin$^+$ structures than were BCP-ALL cells (Figure 4D). In summary, T-ALL cells engraft near blood vessels, bone and nestin$^+$ cells, but BCP-ALL cells predominantly interact with the sinusoidal bone marrow niche (Figure 4E).

B-cell acute lymphoblastic leukemia cells do not co-localize with transition zones

Perivascular cues are essential for the maintenance of normal hematopoiesis and the vascular niche of HSC has been extensively described.[26-28] We therefore explored whether hematopoietic stem and progenitor cells (HSPC, CD34$^+$ cord blood) and BCP-ALL cells occupy the same niche. Using 3D quantitative imaging we investigated in detail the interactions between leukemic cells or HSPC and recently described transitional zones, a special subtype of vessels (endoglin^{low}endomucin^{high}) forming the intersection between arterioles and sinusoids (Figure 5A, B).[29] We observed direct interactions of healthy HSPC with sinusoids (Q1 and Q4) and transition zones as well

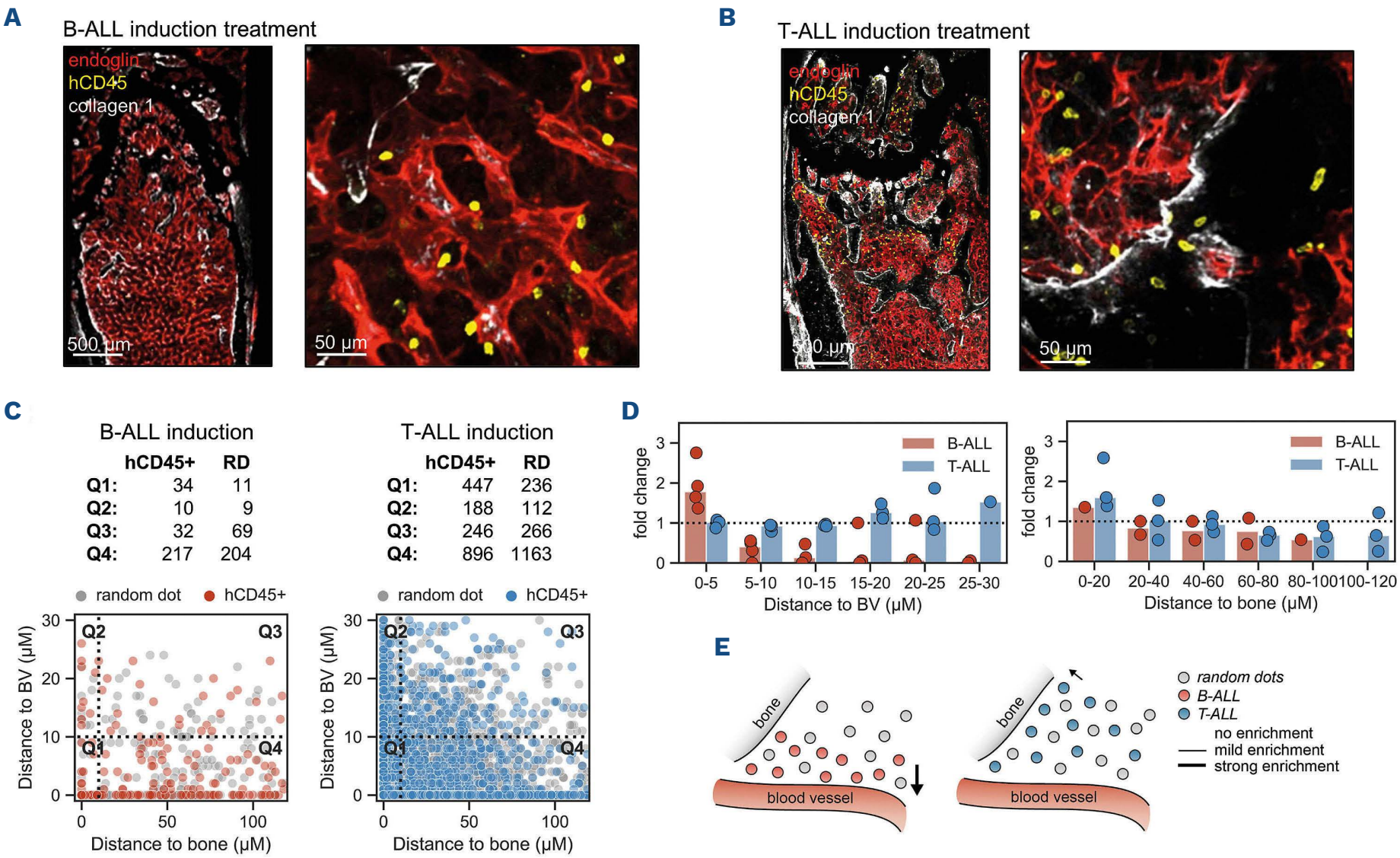

Figure 3. B-cell precursor acute lymphoblastic leukemia and T-acute lymphoblastic leukemia cells exhibit distinct patterns in the bone marrow microenvironment upon chemotherapy. (A, B) Representative maximal projection of a tiled 100-300 µm z-stack confocal image of patient-derived B-cell precursor (BCP) acute lymphoblastic leukemia (ALL) or T-ALL cells upon chemotherapy (A: B-VHR-20; B: T-VHR-09). Scale bars: 500 µm on overviews, 50 µm on zoomed images. Human leukemic cells (CD45$^+$, yellow) in spatial relationship with sinusoids (endoglin$^+$, red) or endosteum (collagen 1a$^+$, white). (C) Distribution of mean distances of BCP-ALL (red, B-R-03, B-SR-21 and B-VHR-24) or T-ALL (blue, T-HR-04, T-VHR-01 and T-VHR-04) cells to the bone and the bone marrow sinusoids after induction treatment (segmented cells n=293 BCP-ALL and n=1,777 T-ALL). (D) Bar chart showing binwise fold-changes of BCP-ALL and T-ALL cells over random dots for distances to blood vessels (left panel) and bone (right panel). (E) Schematic depiction of predilection sites of BCP-ALL (left panel) or T-ALL (right panel) cells in the bone marrow. Q: quartile; BV: blood vessel (bone marrow sinusoid); h: human; RD: random dots.

as enrichment in close proximity, as compared to the distribution of random dots (<10 µm; Q2) (Figure 5C). In contrast, leukemic cells were rarely in contact with transition zones, indicating that BCP-ALL cells specifically interact with the sinusoidal bone marrow niche (<10 µm, Q1 and Q4) (Figure 5C; *Online Supplementary Figure S6*). Hence, transition zones were more likely to be populated by HSPC, which clustered significantly closer to endomucin$^+$ cells and blood vessels than did random dots (<5 µm) (Figure 5D). Consequently, we propose that not all HSPC and BCP-ALL cells share the same vascular niche (Figure 5E).

Chemotherapy and engraftment of leukemic cells induce remodeling of the bone marrow vasculature

Following the application of chemotherapeutic drugs in our *in vivo* model we observed remodeling of bone marrow sinusoids (Figure 6A). In brief, treatment with doxorubicin for 28 days appeared to increase vessel branching, whereas dexamethasone visually dilated vessels. The combination of dexamethasone, doxorubicin and vincristine affected vessel morphology by leading to a denser network of bone marrow sinusoids. Besides chemotherapeutic stress, we observed vessel remodeling under leukemic infiltration. Compared to early engraftment (Figure 6B), during later stages of leukemia infiltration (Figure 6C) there was a more condensed vasculature. This phenotype was reversible within 4 days after chemotherapy exposure (Figure 6D), suggesting a response that is directly related to leukemic engraftment and chemotherapeutic stress. Overall, re-modeling of the vasculature was stronger in B-ALL than in T-ALL models (*Online Supplementary Figure S7*). These observations underline the stable presence of the perivascular niche and possible supportive interactions of niche cells with leukemic blasts even during chemotherapy.

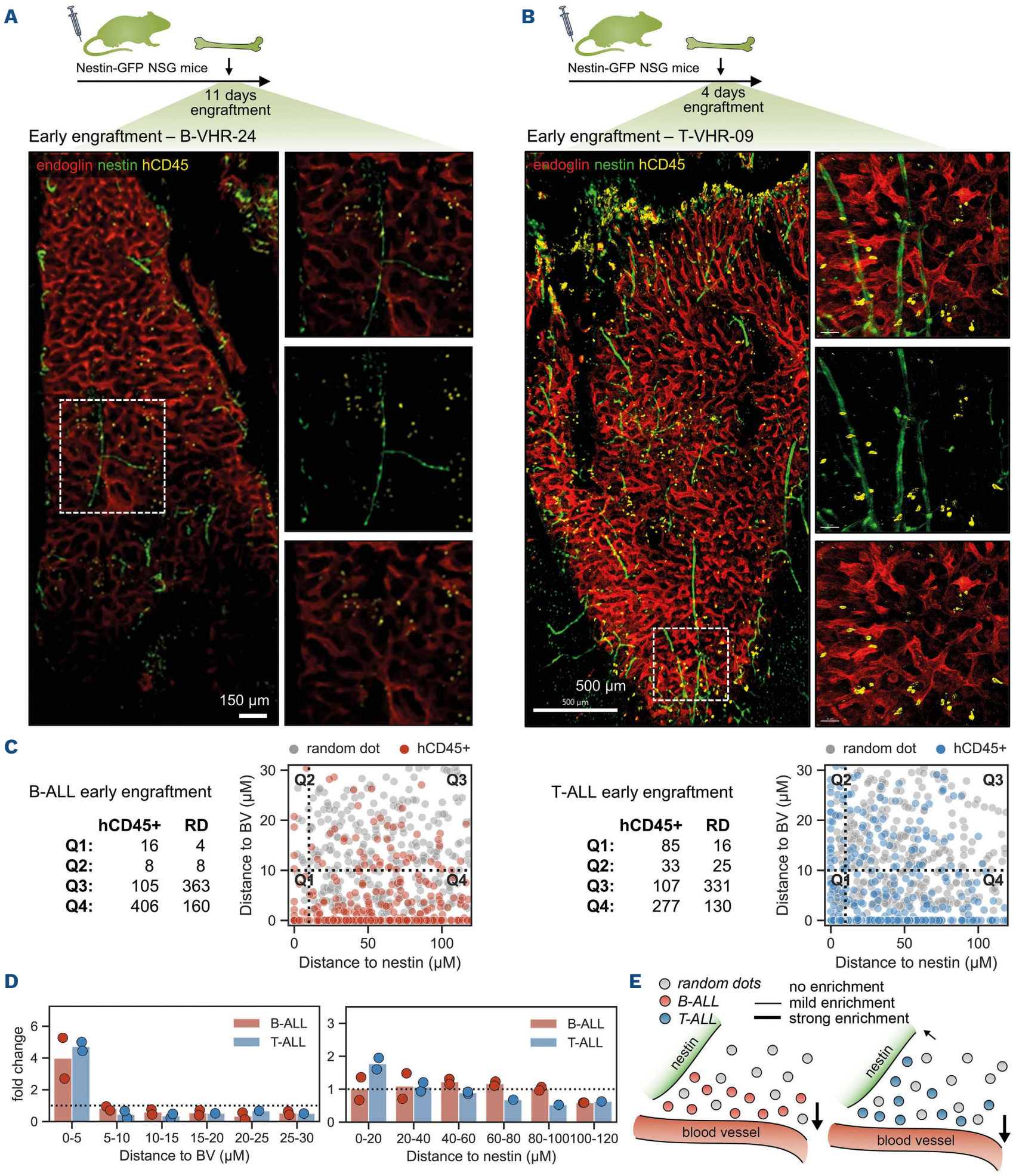

Figure 4. T-cell acute lymphoblastic leukemia cells engraft preferentially in close proximity to nestin-positive cells. (A, B) Representative maximum projection of a tiled 100-300 µm z-stack of the bone marrow of nestin-GFP (green) mice transplanted with cells from B-VHR-24 (hCD45$^+$, yellow) 11 days after transplantation (A) or with cells from T-VHR-09 (hCD45$^+$, yellow) 4 days after transplantation (B). Sinusoids are defined as endoglin$^+$ (scale bars: 150 µm). (C) Distribution of B-cell precursor (BCP) acute lymphoblastic leukemia (ALL) (red, left panel) or T-ALL (blue, right panel) cells depending on their distance from sinusoids and nestin-GFP cells. The graph represents pooled data from two BCP-ALL patients (B-VHR-24 and B-SR-22, segmented cells, n=535) or two T-ALL patients (T-HR-04 and T-VHR-09, segmented cells, n=502). (D) Bar chart representing binwise fold-changes of BCP-ALL and T-ALL cells over random dots for distances from blood vessels (left panel) and nestin$^+$ cells (right panel). (E) Schematic depiction of predilection sites of BCP-ALL (left panel) or T-ALL cells (right panel) in the bone marrow with respect to endoglin$^+$ and nestin$^+$ structures. GFP: green fluorescent protein; Q: quartile; BV: blood vessel (bone marrow sinusoid); h: human; RD: random dots.

Residual resistant acute lymphoblastic leukemia cells maintain their leukemia repopulating capacity and chemotherapy-sensitivity profiles

To explore the transient nature of the resistant phenotype in our MRD model, we verified the ALL cells' function by serial transplantation (Figure 7A) and tested their sensitivity to chemotherapeutic agents *ex vivo*. Residual leukemia cells from very high-risk BCP-ALL and T-ALL were harvested after induction chemotherapy for secondary transplants in NSG mice. These MRD-like (pre-treated) cells recapitulated the leukemia phenotype in secondary transplants with similar kinetics (Figure 7B) compared to the first transplant of untreated cells (Figure 1E), with leukemia cells detectable in the peripheral blood within 20 to 75 days after transplantation. Accordingly, the degree of bone marrow involvement was comparable both at early time-points (1% engraftment in peripheral blood) (Figure 7C) and at later time-points (50% engraftment in peripheral blood) (Figure 7D). Moreover, these MRD-like ALL cells did not show either increased resistance to ALL chemotherapeutic agents in *ex vivo* drug sensitivity testing or a delay in response to treatment *in vivo* (Figure 7E, F; *Online Supplementary Figure S8*). These ob-

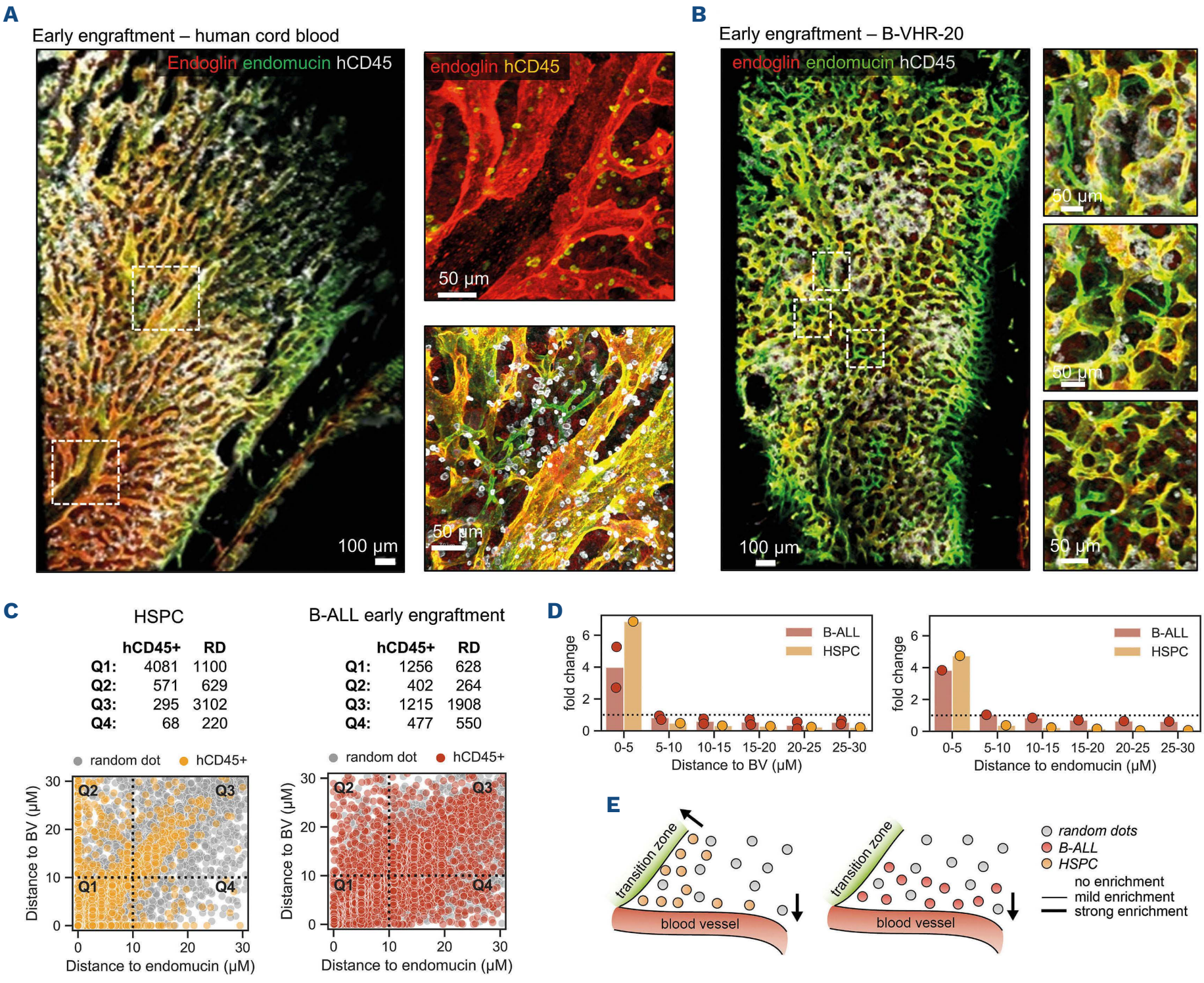

Figure 5. Acute lymphoblastic leukemia (ALL) cells and hematopoietic stem and progenitor cells co-localize with bone marrow sinusoids but ALL cells not with transition zones. (A, B) Representative maximum projection of a tiled 100-300 µm z-stack confocal image of the interactions of hematopoietic stem and progenitor cells (HSPC) (A; hCD45$^+$, yellow/white, CD34$^+$ cord blood cells) or B-cell progenitor (BCP) acute lymphoblastic leukemia (ALL) cells (B; hCD45$^+$, white, B-VHR-20) with sinusoids (endomucin^{low}, green, endoglin$^+$, yellow) and/or the transition zone (endomucin^{high}, green, endoglin^{low}, yellow). (C) Quantitative analysis of distance of HSPC (n=5,015) or BCP-ALL cells (n=3,350) and corresponding random dots from bone marrow sinusoids. (D) Binwise fold-changes of BCP-ALL cells and HSPC over seeded random dots for distance to blood vessels (left panel) or endomucin (right panel). (E) Schematic presentation of predilection sites of HSPC (left panel) or BCP-ALL cells (right panel) in the bone marrow with respect to endoglin$^+$ and endomucin$^+$ structures. BV: blood vessel (bone marrow sinusoid); h: human; RD: random dots; Q: quartile.

servations indicate that the phenotype associated with resistance to chemotherapy is transient, suggesting a role for interactions between the cells and their microenvironment.

Induction chemotherapy does not select quiescent populations

Induction of a persistent quiescent state has been inferred as the central mechanism for drug resistance in leukemia. To follow subpopulations that would become more quiescent under chemotherapy, we used CFSE to track cells for up to eight cell divisions.[30] PDX ALL cells were stained with CFSE *ex vivo*, transplanted and induction treatment was initiated after a window for stable engraftment. Bone marrow was harvested after either a short period of treatment (3 days) or a long period of treatment (28 days) (Figure 8A). The proportion of CFSE-positive leukemic cells after short-term treatment was slightly higher than that in untreated controls, indicating that chemotherapy transiently selects a subpopulation of cells with decreased proliferative activity (Figure 8B; *Online Supplementary Figure S9*). After induction chemotherapy no CFSE-marked populations could be detected (Figure 8C; *Online Supplementary Figure S9*), and we could not identify the existence of a quiescent subset under these experimental conditions, suggesting that our induction chemotherapy affected proliferative and non-proliferative populations similarly. It has also been proposed that

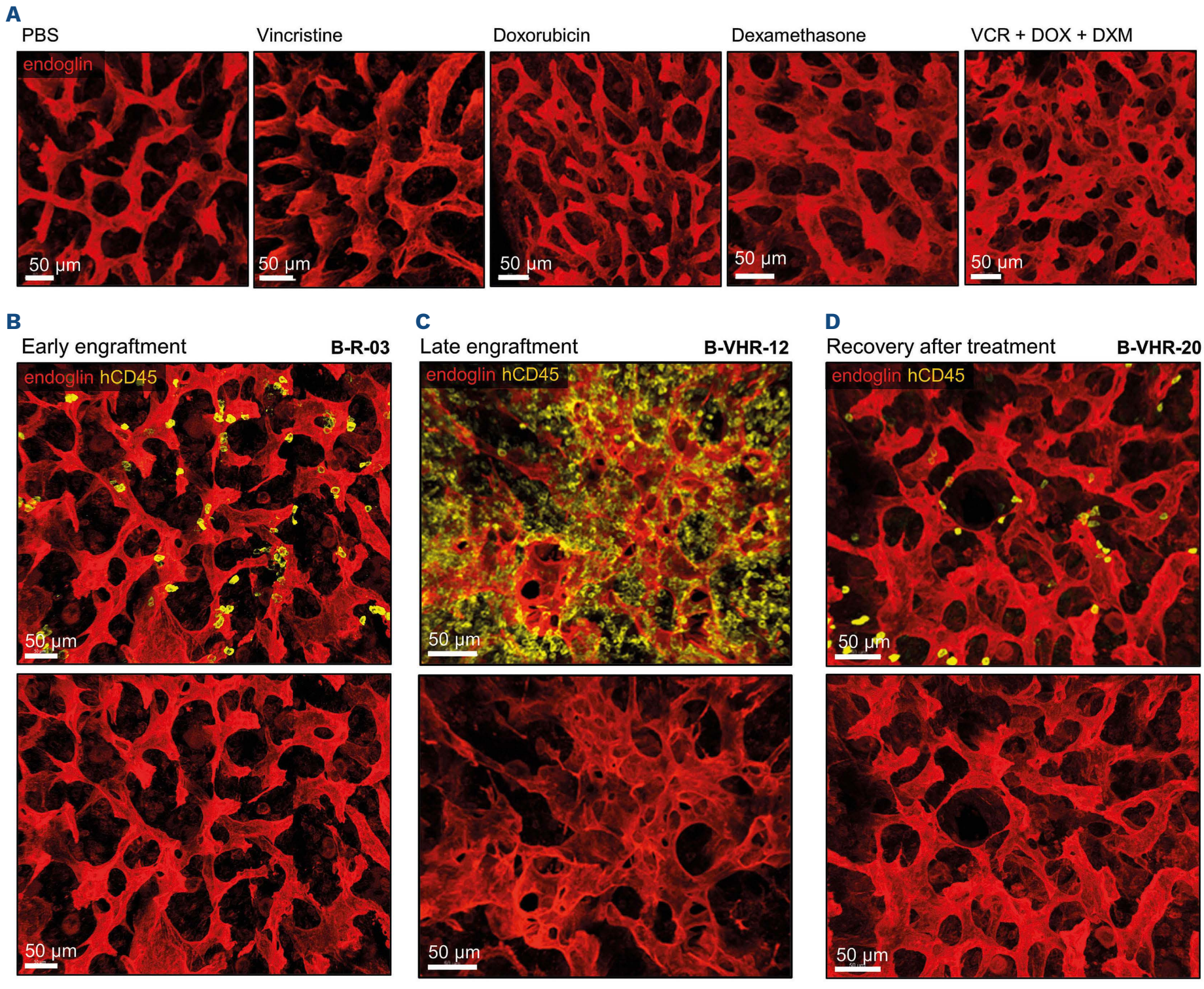

Figure 6. Vascular changes in bone marrow sinusoids upon chemotherapy or engraftment of acute lymphoblastic leukemia cells. (A) Representative maximal projection of tiled 100-300 µm z-stack confocal images of bone marrow sinusoids (endoglin$^+$, red) upon application of phosphate-buffered saline, dexamethasone, vincristine, doxorubicin, or a combination of the three-drug induction therapeutics. (B-D) Effects of early engraftment (B), vascular remodeling at late engraftment (C) and recovery after induction treatment (D) of B-cell precursor acute lymphoblastic leukemia cells (hCD45$^+$, yellow) on the structure of bone marrow sinusoids (endoglin$^+$, red) represented by maximal projection of tiled 100-300 µm z-stack confocal images. PBS: phosphate-buffered saline; h: human; VCR: vincristine; DOX: doxorubicin; DXM: dexamethasone.

quiescent cells reside in vicinity of the endosteum. However, the distribution of CFSE-positive cells after short-term treatment was similar for both BCP-ALL and T-ALL cells, as observed for the total population of hCD45$^+$ cells (Figure 8D-G). After 28 days of chemotherapy, no CFSE-positive cells were observed in the bone marrow in either BCP-ALL or T-ALL cases (Figure 8E, G). Thus our data challenge the notion that the endosteum constitutes the supportive niche for dormant leukemia cells.[31]

Discussion

Here we show that the localization of human BCP-ALL is not random with respect to other bone marrow structures and is distinct from the localization of T-ALL, indicating important functional differences between the two ALL lineage subtypes. BCP-ALL cells survive a typical induction chemotherapy regimen in a sinusoidal context, which is reminiscent of the reported co-localization of pro-B cells and early hematopoietic progenitors in this perisinusoidal space.[32] We confirmed that these sites were distinct from the transition zones and nestin$^+$ arteriole-associated pericytes that have been implicated in the control of HSC quiescence.[6] Recent studies of the murine bone marrow microenvironment identified that niche-associated factors in sinusoidal endothelial cells and perivascular stromal cells modulate HSPC. Loss of the endothelial-specific Notch ligand DLL4 skewed HSPC to a more myeloid gene expression profile with loss of IL-7R-positive common

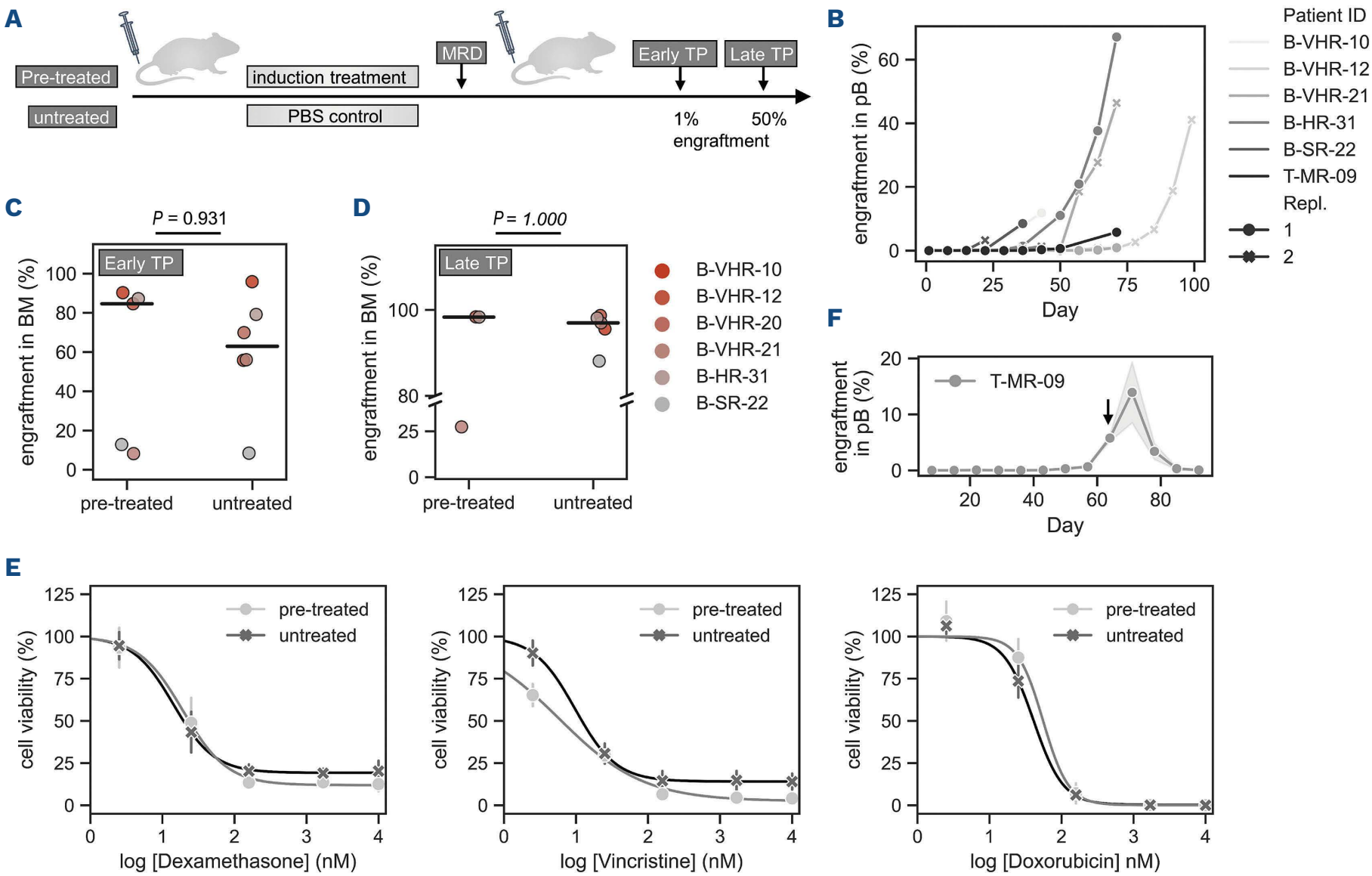

Figure 7. Engraftment properties and response of chemotherapy-resistant acute lymphoblastic leukemia cells to chemotherapeutic drugs. (A) Schematic representation of the transplantation model of minimal residual disease. (B) Flow cytometry analysis of engraftment kinetics in peripheral blood of re-transplanted acute lymphoblastic leukemia (ALL) cells harvested from the bone marrow of mice treated with combination chemotherapy from patients B-VHR-12, B-VHR-10, B-VHR-21, B-SR-22, B-HR-31 and T-MR-09. (C, D) Levels of human cell engraftment in mouse bone marrow at 1% engraftment in peripheral blood (early time-point, C) or 50% engraftment in peripheral blood (late time-point, D) upon transplantation of untreated ALL cells *versus* pre-treated ALL cells resistant to *in vivo* induction treatment and measured by flow cytometry analysis for patients B-VHR-12, B-VHR-10, B-VHR-21, B-SR-22 and B-HR-31. Medians were compared using an unpaired two-tailed Mann-Whitney U test. (E) Drug response profiles of untreated ALL cells *versus* pre-treated ALL cells to *ex vivo* exposure to dexamethasone, vincristine or doxorubicin (9 technical replicates with mean ± standard deviation of B-VHR-20). (F) Flow cytometry analysis of engraftment kinetics in peripheral blood of secondary transplants of ALL cells harvested from the bone marrow of mice treated with combination chemotherapy for 4 weeks from patient T-MR-09 that were treated again with the same combination chemotherapy (therapy start indicated by the black arrow). PBS: phosphate-buffered saline; MRD: minimal residual disease; TP: time-point; pB: peripheral blood; BM: bone marrow.

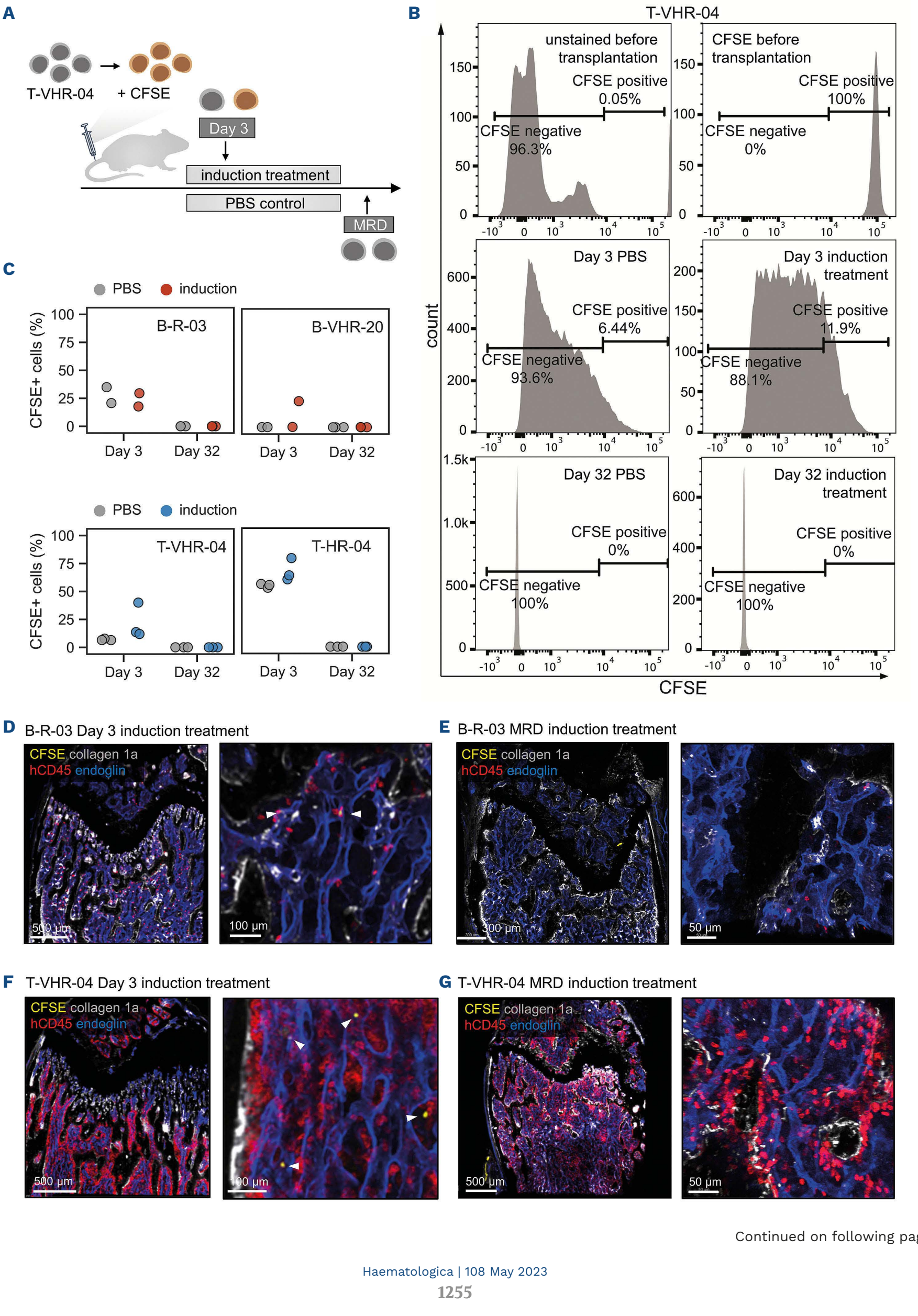

Continued on following page.

Figure 8. Induction chemotherapy increases a transient, slowly proliferating subpopulation of leukemic cells, but does not induce quiescence. (A) Schematic representation of NSG mice transplanted with patient-derived xenograft samples, labeled with 5(6)-carboxyfluorescein diacetate N-succinimidyl ester (CSFE), which were treated with either induction chemotherapy or a 3-day schedule of vincristine and doxorubicin on day 1 and dexamethasone on days 1-3. (B) Gating strategy of leukemia cells in the mouse bone marrow for flow cytometry analysis of $CFSE^+$ or $CFSE^-$ cells after short- or long-term treatment. (C) Quantification of total leukemic burden in femoral bone marrow of patient-derived xenografts of B-cell precursor (BCP) acute lymphoblastic leukemia (ALL) and T-ALL and analysis of proportions of $CFSE^+$ and $CFSE^-$ cells in the $hCD45^+$ cell population in the bone marrow after 3 days of chemotherapy or day 32 after chemotherapy. The data represented are from three animals transplanted with the patient-derived xenograft. (D-G) Representative maximum projection of tiled 100-300 μm z-stack confocal images of $CFSE^+$ BCP-ALL (B-R-03) or T-ALL (T-VHR-04) cells (double positive for CFSE in yellow and hCD45 in red, arrowheads) in the bone marrow of the femur after 3 days of chemotherapy (D and F) or day 32 after chemotherapy (E and G). Sinusoids are defined as $endoglin^+$ (blue), endosteum as $collagen\ 1a^+$ (white). PBS: phosphate-buffered saline; h: human; MRD: minimal residual disease.

lymphoid progenitors cells.[33] Mesenchymal stem cell lineage trajectories were identified in the perivascular space, which expresses different hematopoietic cytokines including CXCL12, SCF and IL-7,[33,34] with further evidence for modulation of B-cell progenitors.[32] These niche-associated factors may contribute to leukemia initiation and progression. Further perturbations of the bone marrow immune microenvironment by B-ALL were detected in human samples, revealing the expansion of non-classical $Ly6C^-$, CSFR1, $CD16^+$ monocytes that depend on vascular-endothelial signaling and upregulate genes involved with vasculo-endothelial interactions. Interference with the CSFR1 receptor synergized with nilotinib in a mouse model of *BCR-ABL*-positive ALL, supporting a role for abnormal interactions in the perisinusoidal niche in ALL.[35]

Reproducible detection of BCP-ALL MRD in the perisinusoidal niche also contradicts a broadly discussed report by Ebinger *et al.*,[15] who proposed a model of resistance based on the persistence of a non-dividing endosteal BCP-ALL population after selection by chemotherapy. We have not been able to detect this endosteal MRD population. However, our data indicate that the MRD cells likely persist in a reversible and transient drug-tolerant state. Moreover, it was observed that leukemic cells are imprinted by specific cell types of the bone marrow microenvironment leading to transitory states of chemoresistance.[36,37] The diverging observations may arise from the selection of different chemotherapeutic agents in the experiments or resolution of the imaging techniques. Indeed, ALL cells compete with HSC in the vicinity of sinusoidal endothelial cells,[12] where the majority of HSC, dormant or cycling, were localized.[10,38] We found that ALL cells overlap only with the non-arteriolar HSC niche. Isolation of niche components for single-cell analysis remains challenging, as flow cytometry-based assays massively underestimate the dense mesh of sinusoidal and CXCL12-expressing mesenchymal cells in the bone marrow when compared to quantitative 3D imaging-based studies.[39,40] Furthermore, we show that this sinusoidal space is maintained even after massive leukemia progression. We confirm transient alternations in cellular endothelial morphology suggestive of stress response and transient expansion of an adipocytic cluster, as detected by others.[13] Dynamic changes of the bone marrow microenvironment may have functional implications for the leukemic cells. T-ALL cells derived from distal adipocytic-rich bone marrow in mouse models demonstrated a higher intrinsic resistance.[38] Adipocytic enrichment in the bone marrow may restrict the proliferative capacity and induce transcriptomic changes of ALL cells leading to chemoresistance.[39,40]

Our results also reconcile important observations made with models of T-ALL.[17] *In vivo* imaging of NOTCH-induced murine T-ALL and T-ALL PDX revealed that T-ALL cells survive combination chemotherapy with increased motility and without any evidence of a quiescent MRD subpopulation and with a predilection for endosteal regions, resulting in rapid loss of osteoblasts, challenging the notion of a restricted niche for T-ALL.[17] Thus niche heterogeneity may reflect differences in functional dependencies in ALL. Given the impact of CXCL12 disruption in endothelial cells for T-ALL in mouse models, interactions in the perisinusoidal space remain relevant.[42,43] This complexity extends to extramedullary sites and can evolve. For example, transgenic expression of the IL-7 receptor in mice leads first to thymic deregulation with malignant evolution in a phenotype that eventually involves the bone marrow.[44] Our results point to heterogeneity in extramedullary MRD, also involving secondary lymphoid organs, which is consistent with the heterogeneity of extramedullary involvement in ALL in the clinic.[45] Additional heterogeneity of structural and metabolic differences occurs at different sites in the body including alterations with aging.[46,47] Integrating imaging approaches and genetic and transcriptomic sequencing analyses[48] at single-cell resolution with molecular interactome maps in normal HSC have revealed dynamic relationships.[33,34,49,50]

In conclusion, specific differences in the localization of leukemic cells upon engraftment and chemotherapy exist between BCP-ALL and T-ALL, suggesting the existence of sites of predilection in the bone marrow microenvironment. More studies are needed to elucidate the functional consequences of niche heterogeneity on leukemia biology and their therapeutic implications. Our observations warrant further dissection of the peri-sinusoidal niche.

Disclosures

No conflicts of interest to disclose.

Contributions

MJB, LB, DC, GZ and IJV designed and carried out experiments. MJB, LB, DC, GZ and FDS analyzed data. MJB, LB, DC, GZ, IJV and BM performed and supported the xenograft experiments. DC and GZ performed most of the xenograft experiments and collected the imaging data. LB established the 3D imaging protocols. AZ, CN-A and UZ provided technical support and data interpretation for the 3D microscopy. MK wrote the Matlab scripts. MK, LK, YZ and TS contributed to image processing and analysis. BB and J-PB supervised the study; MJB, LB, DC, GZ, FDS, BB and J-PB wrote the manuscript. All authors approved the final version of the manuscript.

Acknowledgments

The authors would like to thank Jasper de Boer for providing the pSLIG plasmid, Sander Botter for his support during the establishment of the bioluminescence imaging protocol and Samanta Kisele for support with the mouse studies. We are grateful to Dominique Bonnet and Diana Passaro, who kindly provided nestin-GFP NSG mice. We thank Zsofia Kovacs, Elisabeth Rushing and Anna Rinaldi for support with magnetic resonance imaging and histopathology analyses of the mouse brain. We also acknowledge the assistance of the Center for Microscopy and Image Analysis of the University of Zürich during image acquisition.

Funding

This study was supported by the Swiss National Science Foundation (310030-182269 and 310030-156407), an SNF Sinergia grant (186271), the EU horizon 2020 ITCC-P4 project, the Novartis Foundation for Biomedical Research, the Stiftung Kinderkrebsforschung Schweiz and the Swiss Pediatric Hematology and Oncology SPHO Biobank Network.

Data-sharing statement

The data supporting the findings of this study are available upon request to the author for correspondence.

References

1. Colmone A, Amorim M, Pontier AL, Wang S, Jablonski E, Sipkins DA. Leukemic cells create bone marrow niches that disrupt the behavior of normal hematopoietic progenitor cells. Science. 2008;322(5909):1861-1865.
2. De Bie J, Demeyer S, Alberti-Servera L, et al. Single-cell sequencing reveals the origin and the order of mutation acquisition in T-cell acute lymphoblastic leukemia. Leukemia. 2018;32(6):1358-1369.
3. Schumich A, Maurer-Granofszky M, Attarbaschi A, et al. Flow-cytometric minimal residual disease monitoring in blood predicts relapse risk in pediatric B-cell precursor acute lymphoblastic leukemia in trial AIEOP-BFM-ALL 2000. Pediatr Blood Cancer. 2019;66(5):e27590.
4. Hanahan D, Coussens LM. Accessories to the crime: functions of cells recruited to the tumor microenvironment. Cancer Cell. 2012;21(3):309-322.
5. Taichman R, Reilly M, Emerson S. Human osteoblasts support human hematopoietic progenitor cells in vitro bone marrow cultures. Blood. 1996;87(2):518-524.
6. Kunisaki Y, Bruns I, Scheiermann C, et al. Arteriolar niches maintain haematopoietic stem cell quiescence. Nature. 2013;502(7473):637-643.
7. Asada N, Kunisaki Y, Pierce H, et al. Differential cytokine contributions of perivascular haematopoietic stem cell niches. Nat Cell Biol. 2017;19(3):214-223.
8. Yamazaki S, Ema H, Karlsson G, et al. Nonmyelinating Schwann cells maintain hematopoietic stem cell hibernation in the bone marrow niche. Cell. 2011;147(5):1146-1158.
9. Nguyen TS, Lapidot T, Ruf W. Extravascular coagulation in hematopoietic stem and progenitor cell regulation. Blood. 2018;132(2):123-131.
10. Kokkaliaris KD, Kunz L, Cabezas-Wallscheid N, et al. Adult blood stem cell localization reflects the abundance of reported bone marrow niche cell types and their combinations. Blood. 2020;136(20):2296-2307.
11. Itkin T, Gur-Cohen S, Spencer JA, et al. Distinct bone marrow blood vessels differentially regulate haematopoiesis. Nature. 2016;532(7599):323-328.
12. Sipkins DA, Wei X, Wu JW, et al. In vivo imaging of specialized bone marrow endothelial microdomains for tumour engraftment. Nature. 2005;435(7044):969-973.
13. Duan C-W, Shi J, Chen J, et al. Leukemia propagating cells rebuild an evolving niche in response to therapy. Cancer Cell. 2014;25(6):778-793.
14. Veiga JP, Costa LF, Sallan SE, Nadler LM, Cardoso AA. Leukemia-stimulated bone marrow endothelium promotes leukemia cell survival. Exp Hematol. 2006;34(5):610-621.
15. Ebinger S, Özdemir EZ, Ziegenhain C, et al. Characterization of rare, dormant, and therapy-resistant cells in acute lymphoblastic leukemia. Cancer Cell. 2016;30(6):849-862.
16. van der Velden V, Jacobs D, Wijkhuijs A, et al. Minimal residual disease levels in bone marrow and peripheral blood are comparable in children with T cell acute lymphoblastic leukemia (ALL), but not in precursor-B-ALL. Leukemia. 2002;16(8):1432-1436.
17. Hawkins ED, Duarte D, Akinduro O, et al. T-cell acute leukaemia exhibits dynamic interactions with bone marrow microenvironments. Nature. 2016;538(7626):518-522.
18. Fischer U, Forster M, Rinaldi A, et al. Genomics and drug profiling of fatal TCF3-HLF–positive acute lymphoblastic leukemia identifies recurrent mutation patterns and therapeutic options. Nat Genet. 2015;47(9):1020-1029.
19. Richter-Pechańska P, Kunz JB, Bornhauser B, et al. PDX models recapitulate the genetic and epigenetic landscape of pediatric T-cell leukemia. EMBO Mol Med. 2018;10(12):e9443.
20. Mishchenko Y. A fast algorithm for computation of discrete Euclidean distance transform in three or more dimensions on vector processing architectures. Signal Image Video P. 2015;9(1):19-27.
21. Coutu DL, Kokkaliaris KD, Kunz L, Schroeder T. Multicolor quantitative confocal imaging cytometry. Nat Methods. 2018;15(1):39-46.
22. Zinngrebe J, Debatin K-M, Fischer-Posovszky P. Adipocytes in hematopoiesis and acute leukemia: friends, enemies, or

innocent bystanders? Leukemia. 2020;34(9):2305-2316.
23. Williams MTS, Yousafzai YM, Elder A, et al. The ability to cross the blood–cerebrospinal fluid barrier is a generic property of acute lymphoblastic leukemia blasts. Blood. 2016;127(16):1998-2006.
24. Bartram J, Goulden N, Wright G, et al. High throughput sequencing in acute lymphoblastic leukemia reveals clonal architecture of central nervous system and bone marrow compartments. Haematologica. 2018;103(3):e110-e114.
25. Coutu DL, Kokkaliaris KD, Kunz L, Schroeder T. Three-dimensional map of nonhematopoietic bone and bone-marrow cells and molecules. Nat Biotechnol. 2017;35(35):1202-1210.
26. Kopp H-G, Hooper AT, Avecilla ST, Rafii S. Functional heterogeneity of the bone marrow vascular niche. Ann N Y Acad Sci. 2009;1176(1):47-54.
27. Morrison SJ, Scadden DT. The bone marrow niche for haematopoietic stem cells. Nature. 2014;505(7483):327-334.
28. Calvi LM, Link DC. The hematopoietic stem cell niche in homeostasis and disease. Blood. 2015;126(22):2443-2451.
29. Kusumbe AP, Ramasamy SK, Itkin T, et al. Age-dependent modulation of vascular niches for haematopoietic stem cells. Nature. 2016;532(7599):380.
30. Marturano-Kruik A, Nava MM, Yeager K, et al. Human bone perivascular niche-on-a-chip for studying metastatic colonization. Proc Natl Acad Sci U S A. 2018;115(6):1256-1261.
31. Ebinger S, Özdemir EZ, Ziegenhain C, et al. Characterization of rare, dormant, and therapy-resistant cells in acute lymphoblastic leukemia. Cancer Cell. 2016;30(6):849-862.
32. Balzano M, De Grandis M, Vu Manh T-P, et al. Nidogen-1 contributes to the interaction network involved in pro-B cell retention in the peri-sinusoidal hematopoietic stem cell niche. Cell Rep. 2019;26(12):3257-3271.
33. Tikhonova AN, Dolgalev I, Hu H, et al. The bone marrow microenvironment at single-cell resolution. Nature. 2019;569(7755):222-228.
34. Baryawno N, Przybylski D, Kowalczyk MS, et al. A cellular taxonomy of the bone marrow stroma in homeostasis and leukemia. Cell. 2019;177(7):1915-1932.
35. Witkowski MT, Dolgalev I, Evensen NA, et al. Extensive remodeling of the immune microenvironment in B cell acute lymphoblastic leukemia. Cancer Cell. 2020;37(6):867-882.
36. Cahu X, Calvo J, Poglio S, et al. Bone marrow sites differently imprint dormancy and chemoresistance to T-cell acute lymphoblastic leukemia. Blood Adv. 2017;1(20):1760-1772.
37. Heydt Q, Xintaropoulou C, Clear A, et al. Adipocytes disrupt the translational programme of acute lymphoblastic leukaemia to favour tumour survival and persistence. Nat Commun. 2021;12(1):5507.
38. Acar M, Kocherlakota KS, Murphy MM, et al. Deep imaging of bone marrow shows non-dividing stem cells are mainly perisinusoidal. Nature. 2015;526(7571):126-130.
39. Gomariz A, Helbling PM, Isringhausen S, et al. Quantitative spatial analysis of haematopoiesis-regulating stromal cells in the bone marrow microenvironment by 3D microscopy. Nat Commun. 2018;9(1):2532.
40. Kunz L, Schroeder T. A 3D tissue-wide digital imaging pipeline for quantitation of secreted molecules shows absence of CXCL12 gradients in bone marrow. Cell Stem Cell. 2019;25(6):846-854.
41. Hawkins ED, Duarte D, Akinduro O, et al. T-cell acute leukaemia exhibits dynamic interactions with bone marrow microenvironments. Nature. 2016;538(7626):518.
42. Pitt LA, Tikhonova AN, Hu H, et al. CXCL12-producing vascular endothelial niches control acute T cell leukemia maintenance. Cancer Cell. 2015;27(6):755-768.
43. Passaro D, Di Tullio A, Abarrategi A, et al. Increased vascular permeability in the bone marrow microenvironment contributes to disease progression and drug response in acute myeloid leukemia. Cancer Cell. 2017;32(3):324-341.
44. Silva AP, Almeida ARM, Cachucho A, et al. Overexpression of wild type IL-7Rα promotes T-cell acute lymphoblastic leukemia/lymphoma. Blood. 2021;138(12):1040-1052.
45. Bhojwani D, Pui C-H. Relapsed childhood acute lymphoblastic leukaemia. Lancet Oncol. 2013;14(6):e205-e217.
46. Calvo J, Fahy L, Uzan B, Pflumio F. Desperately seeking a home marrow niche for T-cell acute lymphoblastic leukaemia. Adv Biol Regul. 2019;74:100640.
47. Lassailly F, Foster K, Lopez-Onieva L, Currie E, Bonnet D. Multimodal imaging reveals structural and functional heterogeneity in different bone marrow compartments: functional implications on hematopoietic stem cells. Blood. 2013;122(10):1730-1740.
48. Behrmann L, Wellbrock J, Fiedler W. The bone marrow stromal niche: a therapeutic target of hematological myeloid malignancies. Expert Opin Ther Targets. 2020;24(5):451-462.
49. Baccin C, Al-Sabah J, Velten L, et al. Combined single-cell and spatial transcriptomics reveal the molecular, cellular and spatial bone marrow niche organization. Nat Cell Biol. 2020;22(1):38-48.
50. Mende N, Jolly A, Percin GI, et al. Prospective isolation of nonhematopoietic cells of the niche and their differential molecular interactions with HSCs. Blood. 2019;134(15):1214-1226.